*Can. J. Remote Sensing*, Vol. 34, No. 2, pp. 100–112, 2008

# InSAR detects possible thaw settlement in the Alaskan Arctic Coastal Plain[1]

R.P. Rykhus and Z. Lu

**Abstract.** Satellite interferometric synthetic aperture radar (InSAR) has proven to be an effective tool for monitoring surface deformation from volcanoes, earthquakes, landslides, and groundwater withdrawal. This paper seeks to expand the list of applications of InSAR data to include monitoring subsidence possibly associated with thaw settlement over the Alaskan Arctic Coastal Plain. To test our hypothesis that InSAR data are sufficiently sensitive to detect subsidence associated with thaw settlement, we acquired all Japanese Earth Resources Satellite-1 (JERS-1) L-band data available for the summers of 1996, 1997, and 1998 over two sites on the Alaska North Slope. The least amount of subsidence for both study sites was detected in the interferograms covering the summer of 1996 (2–3 cm), interferograms from 1997 and 1998 revealed that about 3 cm of subsidence occurred at the northern Cache One Lake site, and about 5 cm of subsidence was detected at the southern Kaparuk River site. These preliminary results illustrate the capacity of the L-band (24 cm) wavelength JERS-1 radar data to penetrate the short Arctic vegetation to monitor subsidence possibly associated with thaw settlement of the active layer and (or) other hydrologic changes over relatively large areas.

**Résumé.** L'interférométrie satellite par radar à synthèse d'ouverture (InSAR) s'est révélée être un outil efficace pour le suivi de la déformation de surface des volcans, des tremblements de terre, glissements de terrain et nappes phréatiques. Le présent document vise à élargir le champ d'application de l'InSAR en y incluant le suivi de l'affaissement de la plaine cotière arctique d'Alsaka, affaissement sans doute lié au réchauffement de la plaine. Pour valider l'hypothèse selon laquelle les données InSAR sont suffisamment sensible pour détecter l'affaissement associée au rechauffement, nous avons acquis la totalité des données JERS-1 (« Japanese Earth Resources Satellite-1 »), bande L disponibles pour les étés 1996, 1997 et 1998, sur deux sites du versant nord de l'Alaska. L'affaissement minimum pour les deux sites d'étude a été détecté dans les interférogrammes couvrant l'été 1996 (2–3 cm), tandis que les interférogrammes de 1997 et 1998 ont révélé un affaissement de 3 cm au nord du lac Cache One, et un de 5 cm au sud du fleuve Kaparuk. Ces résultats préliminaires illustrent la capacité de la bande L (24 cm de longueur d'onde) de JERS-1 à pénétrer à travers la fine couche de végétation arctique pour ainsi suivre l'affaissement eventuellement associé au rechauffement de la couche active et (ou) d'autres changements hydrologiques sur de plus grandes superficies.

## Introduction

There has been considerable speculation about the possibility of a positive feedback in global warming processes in the Arctic, in which increased warming would lead to increased thawing of the permafrost, which would increase the release of the greenhouse gases carbon dioxide ($CO_2$) and methane ($CH_4$), resulting in even more warming (Frohn et al., 2005; Oechel et al., 2000; Tarnocai, 2004; Walter et al., 2006). In northern latitudes, global warming is being expressed as a lengthening of the growing season, as evidenced by disappearing permafrost and infrastructure damage (Lawrence and Slater, 2005; Nelson et al., 2002). The rate and magnitude of warming in northern latitudes are of special concern given the extensive permafrost, the high carbon densities in the soil, and the potential for positive feedbacks to the global system. A better understanding of the distribution of permafrost thaw patterns and its changes is critical for the realistic modeling of ecosystem performance.

By definition, permafrost is any soil or rock material that continuously remains below 0 °C for 2 or more years (*Arctic geobotanical atlas*, www.arcticatlas.org). The 2-year minimum stipulation is meant to exclude from the definition the overlying ground surface layer, which freezes every winter and thaws every summer. This layer is commonly called the active layer. Approximately 24% of the Northern Hemisphere land mass is underlain by permafrost (Zhang et al., 1999). The hydrology of northern latitudes underlain by permafrost is characterized by the barrier that permafrost poses to the vertical movement of water (Hinzman et al., 1991; Kane et al., 1996; Lawrence and

Received 30 November 2008. Accepted 7 May 2008. Published on the *Canadian Journal of Remote Sensing* Web site at http://pubs.nrc-cnrc.gc.ca/cjrs on 25 July 2008.

**R.P. Rykhus.**[2] Science Applications International Corporation (SAIC), Center for Earth Resources Observation and Science (EROS), US Geological Survey (USGS), 47914 252nd Street, Sioux Falls, SD 57198, USA.

**Z. Lu.** Cascades Volcano Observatory, US Geological Survey (USGS), 1300 SE Cardinal Court, Vancouver, WA 98683, USA.

[1]Work performed under US Geological Survey (USGS) contract 03CRCN0001.
[2]Corresponding author (e-mail: rykhus@usgs.gov).

 

Slater, 2005; Nelson et al., 2002; Pullman et al., 2007). Permafrost determines surface microtopography (Christensen et al., 2004) and, in the far northern part of Alaska, allows for the formation of many small lakes and drained thaw lake basins (Frohn et al., 2005; Hinkel et al., 2003).

As permafrost thaws, roads and buildings that were built on permafrost are in jeopardy of collapse. Future construction will require new designs that will withstand the thawing process or prevent the continued thawing under the infrastructure. Permafrost thawing and the resulting enhancement of water infiltration and accelerated decomposition of large stores of frozen organic carbon could radically affect ecosystems of the Boreal and Arctic regions (Jorgenson et al., 2001; 2006). Radical changes are evident in areas where the permafrost has fully thawed (Christensen et al., 2004); new lakes are forming, and others are draining as the natural percolation of water is altered by the melting soil (Lawrence and Slater, 2005).

### InSAR overview

Interferometric synthetic aperture radar (InSAR) is a relatively new remote sensing technique involving the use of two or more synthetic aperture radar (SAR) images of the surface to detect subtle topographic changes resulting from natural or anthropogenic sources (Lu, 2007; Lu et al., 2005a; 2005c; 2007; Massonnet and Feigl, 1998). InSAR combines the phase information from two or more SAR images of the same area acquired from similar vantage points at different times to produce an interferogram. The interferogram, depicting range changes between the radar satellite and the ground, can be further processed with a digital elevation model (DEM) to detect surface deformation with a horizontal resolution of tens of metres over an area 100 km × 100 km, with centimetre to subcentimetre vertical precision (under favorable conditions). Because SAR operates at microwave wavelengths (from a few centimetres to tens of centimetres) it is able to penetrate clouds and rain during its day and night passes to acquire timely images over cloud-prone Arctic regions.

Interferometry has been used to measure deformation associated with a number of natural and anthropogenic causes. InSAR has successfully been used to monitor volcanic deformation caused by the movement of a magma source located many kilometres beneath the Earth's surface (Lu et al., 2003; 2005b; 2007; Wicks et al., 1998) and deformation caused by earthquakes (Fialko et al., 2002; Lu et al., 2005c). Other researchers have shown that InSAR is able to detect and measure deformation caused by the withdrawal and recharge of groundwater (Bawden et al., 2001). More recently, InSAR has proven useful for measuring changes in water levels in swamp forests (Lu et al., 2005a). Through this research we attempt to expand the list of InSAR applications to include the measurement of seasonal subsidence possibly associated with the thaw settlement of Arctic lands underlain by permafrost.

### Past studies

Since permafrost degradation may lead to significant ground surface subsidence, it is of paramount importance to understand land surface deformation induced by changing permafrost over northern Alaska. Our objective is to investigate whether all-weather Japanese Earth Resources Satellite-1 (JERS-1) InSAR images are capable of measuring subtle ground surface deformation that may be related to the seasonal thawing of the active layer. A past study using European Earth Resources Satellite (ERS-1) InSAR data reported measuring about 3 cm of uplift related to frost heave during the fall of 1995 (Wang and Li, 1999). To our knowledge, no InSAR-based studies measuring the subsidence caused by thaw settlement have been published. However, other researchers have attempted to measure thaw settlement using short-wavelength C-band radar data without success (C. Werner, personal communication, 2007). A study using differential global positioning system data measured about 4 cm of subsidence near Prudhoe Bay, Alaska, during 2001–2002 and attributed the subsidence to thaw settlement (Little et al., 2003).

Past attempts to detect and monitor the subsidence associated with the seasonal thawing of the active layer were conducted using short-wavelength C-band data. The C-band radar often resulted in poor coherence over the study areas. The objective of this paper is to demonstrate that longer L-band wavelength data are better suited to monitoring deformation in Arctic regions. The L-band JERS-1 data will maintain coherence in the rapidly changing Arctic environment to detect subsidence possibly related to the thawing of the active layer.

## North Slope study site

A large part of the Alaska North Slope, from just south of Prudhoe Bay in the north to the Brooks Range in the south, serves as our overall study site (**Figure 1**). The study site contains a variety of vegetation types typically associated with permafrost (Jorgenson and Heiner, 2004; Walker et al., 1994). According to Jorgenson and Heiner (2004), the dominant vegetation type in our study site is wet sedge tussock tundra. The southern, hillier portion of our study site is underlain by permafrost with a thickness of approximately 250–350 m (Kane et al., 1996). The northern portion of our study area near the Beaufort Sea has a significantly thicker (600 m) layer of permafrost and a thermokarst type of landscape (McNamara et al., 1998) composed of several small lakes and drained thaw lake basins. Topography in the thermokarst landscape is irregular and hummocky, with pits and depressions developed by thaw settlement in an otherwise smooth landscape (Frohn et al., 2005; Hinkel and Nelson, 2003; Hinkel et al., 2001).

The depth of thaw of the active layer is dependent on (*i*) topographic factors such as slope and aspect, (*ii*) climatic factors such as air and ground temperature, (*iii*) hydrologic factors such as the presence of running water (Kane et al., 1996; McNamara et al., 1998), and (*iv*) vegetation type and the thickness of the organic (duff) layer. In the southern uplands,

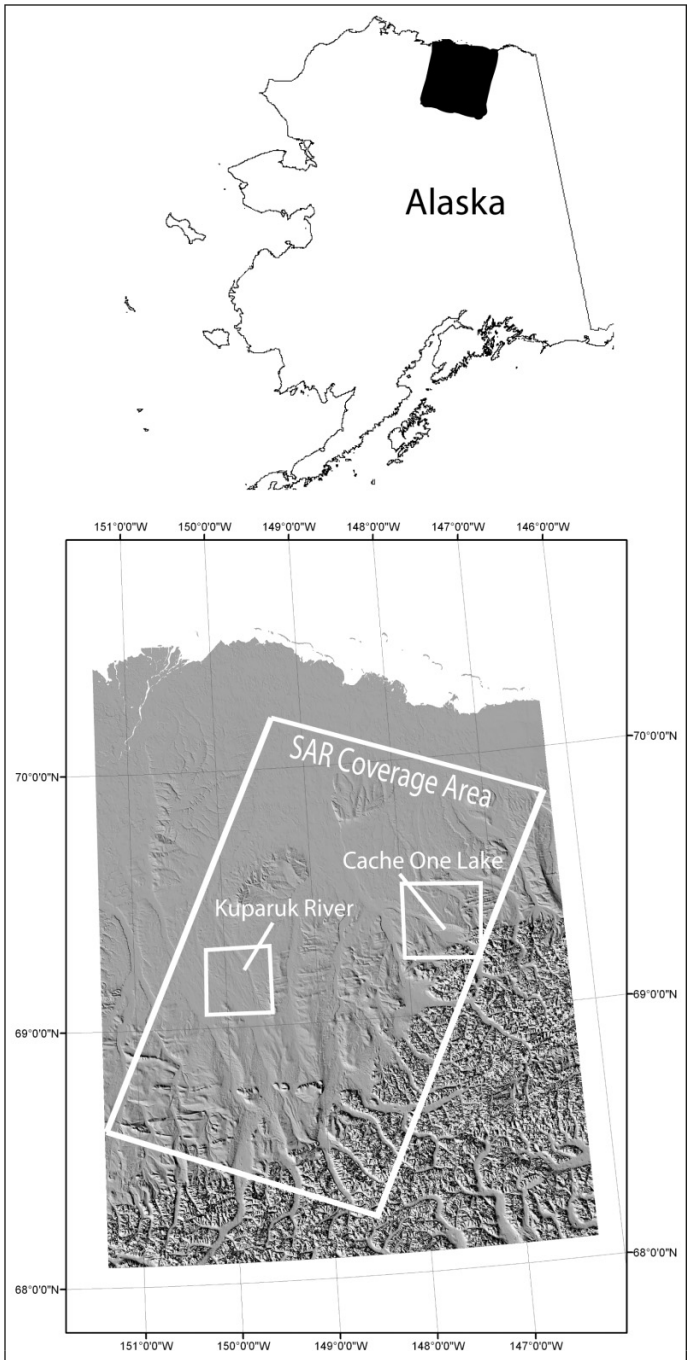


**Figure 1.** Illustration showing the approximate location of the overall study area, the approximate coverage of the four JERS-1 radar data tracks, and the location of the Cache One Lake and Kuparuk River study sites.

the active layer may be as thick as 70 cm; in the northern lowlands, the active layer may be as shallow as 30 cm (Wang and Li, 1999). However, the depth of the active layer can be radically altered by the presence of flowing water. In lowland riverine areas, the continued presence of flowing water and its thermal transmission of heat can lead to active layer thaw depths of approximately 50 cm or more along lowland streams and river channels (Hinkel and Nelson, 2003; Hinzman et al., 1991; Kane et al., 1996; Nelson et al., 1997; 1998). Because of the greater depth of thaw in riverine ecosystems, one may expect there to be greater thaw subsidence in riverine ecoregions than in upland tundra areas (Hinkel and Nelson, 2003; Shiklomanov and Nelson, 1999). We therefore decided to concentrate our efforts to detect changes in elevation to ice-rich riverine ecosystems where the expected surface subsidence would be greater than that of the surrounding uplands regions.

Because of a banding problem (for a complete discussion see the section titled Ionospheric changes) in the full JERS-1 scenes, and the resulting loss of interferometric coherence, we decided to focus our study on two riverine sites where the radar phase signal appears to be relatively unaffected by the banding problem (**Figure 2**). The Cache One Lake study site, located at 69°18′N latitude and 147°43′W longitude, is located in the eastern portion of the overall study area (**Figure 1**). The Cache One Lake site is dominated by two well-defined riverine areas and is located in the foothills of the Brooks Range. The Cache One Lake site ranges in elevation from ~224 m in the northwest corner to ~1417 m in the southeastern portion of the site (**Figure 3A**). According to Jorgenson and Heiner (2004), the upland areas of the Cache One Lake site are dominated by upland shrubby tussock tundra vegetation, and the well-defined riverine areas are dominated by riverine moist sedge–shrub vegetation (**Figure 3B**). Since the riverine areas in the Cache One Lake site are constrained by topography, we expect the majority of the subsidence to be limited to the two riverine areas.

The second study site, the Kuparuk River site, is located in the southwestern portion of the overall study area, along the Kuparuk River (**Figure 1**). The Kuparuk River site is centered on the point at 68°58′N latitude and 149°33′W longitude. The Kuparuk River study site contains gently rolling terrain that varies in elevation from ~250 m to ~750 m (**Figure 3C**); about 80% of the site is covered with a riverine wetland type of ecosystem (**Figure 3D**) (Jorgenson and Heiner, 2004). The dominant type of vegetation in the riverine areas is a moist sedge–shrub type of vegetation. The Kuparuk River site is treeless and is underlain by a continuous layer of permafrost (Walker et al., 1994). Unlike the Cache One Lake site, the two riverine areas in the Kuparuk River site are not tightly constrained by topography but tend to meander into broad floodplains separated by a rolling hill that extends from north to south across the study area. Located near the center of the Kuparuk River site is a lowland area classified as riverine barrens (Jorgenson and Heiner, 2004). This area appears to be flooded in the spring JERS-1 images but is not flooded in the fall imagery. Along the riverine areas in the Kuparuk River site, the depth of thaw of the active layer is greater than 70 cm (Shiklomanov and Nelson, 1999). The combined area of the two study sites is large enough to test the capabilities of the JERS-1 InSAR data for mapping land surface deformation caused by thaw settlement.

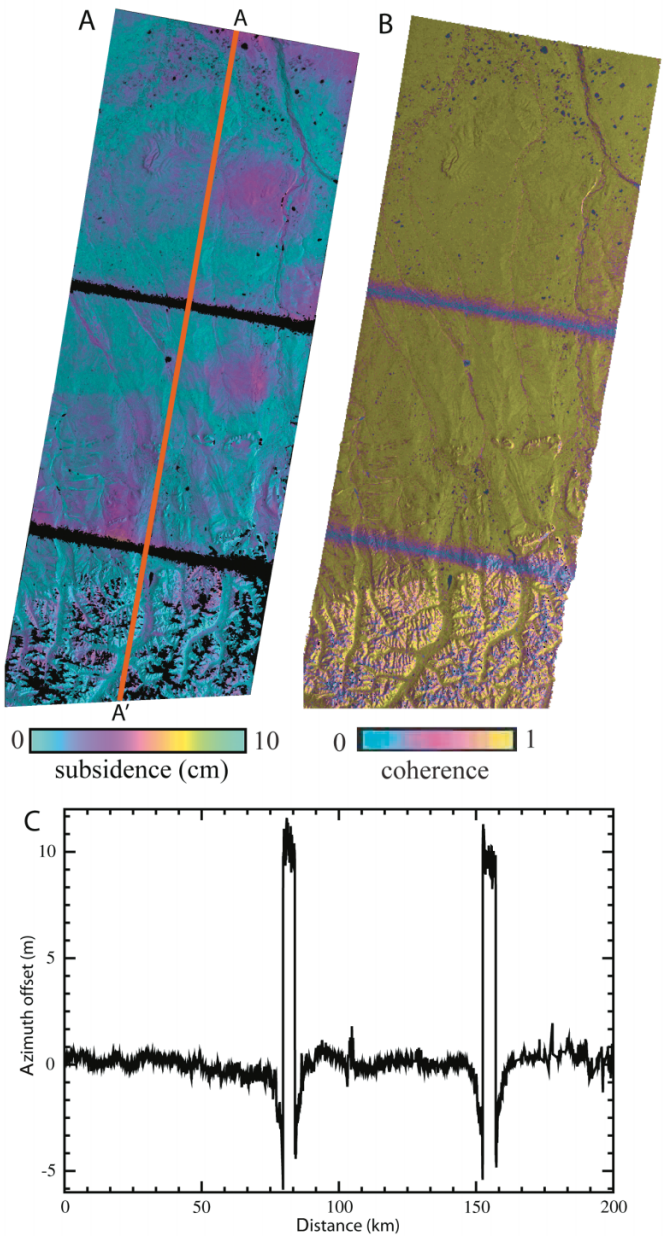


**Figure 2.** (A, B) JERS-1 interferogram and coherence data obtained using the 17 June – 31 July 1996 interferometric pair. (C) The azimuth offsets used to create the interferogram in (A). The change in azimuth offsets is most likely due to ionospheric disturbances during acquisition. Furthermore, the coherence image in (B) illustrates the loss of interferometric coherence over the ionospherically affected zones.

## InSAR data and processing

We obtained SAR images of our study areas suitable to create InSAR pairs for the summers of 1996, 1997, and 1998 to map seasonal land surface deformation over the two study sites. Because longer wavelength L-band SAR penetrates vegetation better than shorter wavelength data (C-band), we obtained 29 L-band JERS-1 scenes over our study site from the Alaska Satellite Facility. Seventeen JERS-1 scenes were used to create 10 interferograms of the study sites (**Table 1**). The remaining 12 scenes were determined to be contaminated by atmospheric and (or) other noise and were not used in the study. At high latitudes, individual JERS-1 scenes from adjacent tracks overlap approximately 70%, thus reducing the temporal repeat pass frequency and increasing the number of InSAR pairs for a given study site. Unfortunately, annual InSAR pairs could not be created because of large baselines and other orbital geometry issues with the JERS-1 data. The subsidence estimates in this study are limited to only the seasonal consequences of the thawing permafrost rather than the subsidence caused by the interannual freeze–thaw cycle and the associated reduction in the volume of the active layer.

### InSAR processing techniques

The US Geological Survey 15 min Alaska DEM (Gesch, 1994) with a specified horizontal accuracy of ~60 m and root mean square vertical error of less than 15 m was used to remove the topographic effects in the interferograms (Massonnet and Feigl, 1998). The resultant topography-removed interferometric phase then contains information related to ground surface deformation, changes in atmospheric conditions, and noise; **Figures 4A**, **4B**, and **4C**, respectively, show that, although the subsidence is somewhat controlled by topography, the DEM successfully removed the topographic effects from the interferograms. If the topographic effects had not been removed, the subsidence would be restricted to areas having the same elevation, and the interferometric fringes would appear like a contour map. The interferogram in **Figure 6G** shows that, although the maximum amount of subsidence does tend to occur in the lowlands, the interferometric fringes do not closely follow the topography because some areas having rather large amounts of subsidence are located on hilltops. Since many factors such as ground temperature and vegetation type are to some degree controlled by topography, the interferograms for the sites will always show some correlation between subsidence and topography (Hinkel et al., 1990).

An interferogram is the complex cross-correlation of two SAR images and measures changes in elevation between image observations. Therefore, InSAR is only capable of providing a snapshot of how the surface changes with respect to elevation between the two observation periods. The amplitude of the cross-correlation, referred to as interferometric coherence, describes the degree to which the two SAR images are correlated. When compared with C-band wavelength radar data, longer wavelength JERS-1 SAR data penetrate farther into the vegetation canopy and are therefore not as affected by changes to the upper portion of the vegetation canopy. The backscatter signal from the JERS-1 sensor should remain coherent under conditions that would cause shorter C-band wavelength SAR sensors like the European Earth Resources Satellite (ERS-1/2) and Canadian RADARSAT-1 sensors to lose coherence. Satellite position and attitude are used to

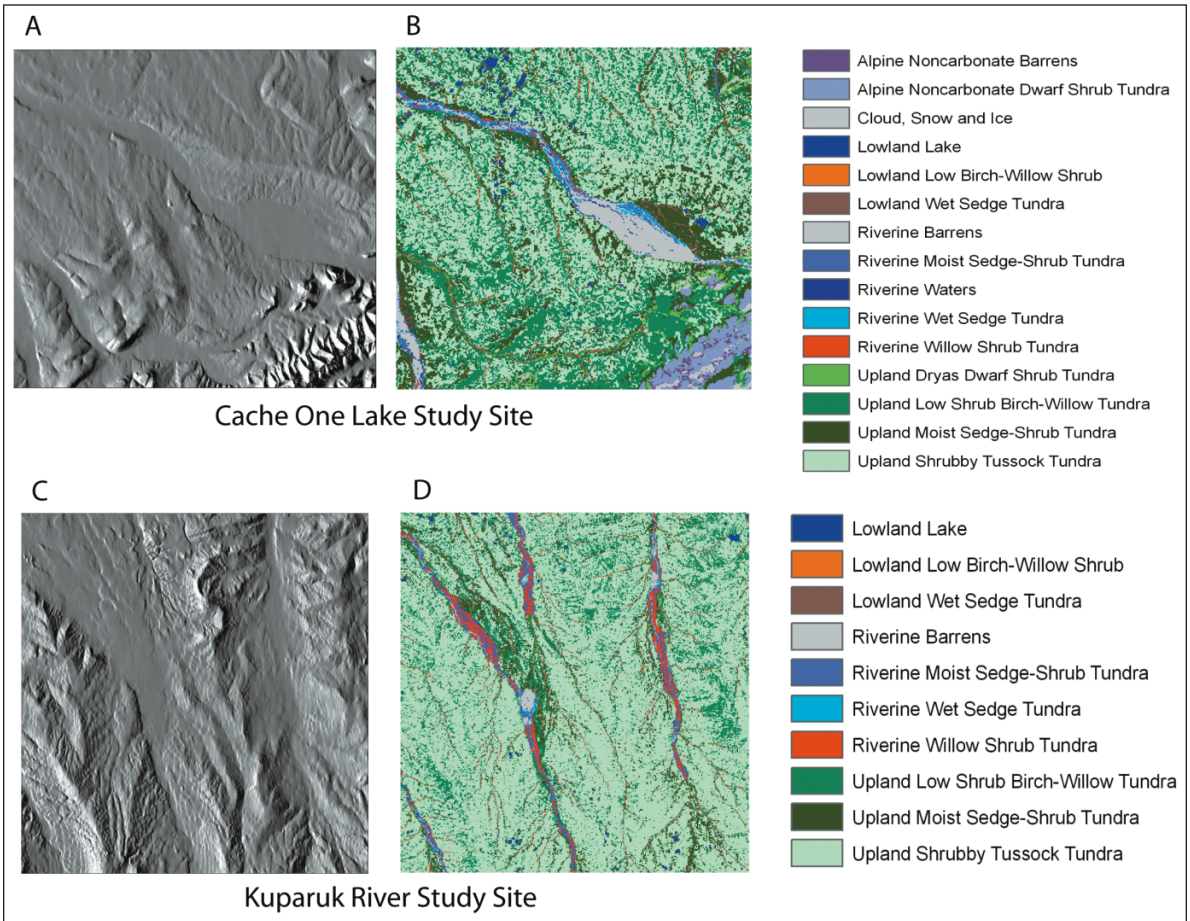


**Figure 3.** Shaded-relief images and land cover information for both the Cache One Lake and Kuparuk River study sites. Comparing land cover types to the deformation in **Figures 5** and **6** reveals that the deformation is not affected by vegetation type, as the subsidence occurs in lowland, riverine, and upland vegetation classes.

remove effects caused by orbital differences between the two passes. Because of the poor accuracy of the position vectors in JERS-1 data, baseline estimates (**Table 1**) are not accurate and can result in long-wavelength artifacts in the final interferogram. To refine JERS-1 baseline estimates, we used the DEM as a constraint to remove artifacts because of the indetermination of the baseline (Rosen et al., 1996). In this approach, the interferometric fringes over the whole region were used in a least-squares approach to determine the baseline vector (Rosen et al., 1996). The resulting interferometric phase values are coded according to a range of colors. A full cycle of colors in the interferogram is often termed a fringe. A single fringe represents a phase change of $2\pi$, which is equivalent to a radar range change of half the radar wavelength, or about 12 cm for the JERS-1 data. In this study the range of colors from cyan–magenta–yellow–green represents about three quarters of a fringe or about 10 cm of deformation. The color order of the fringes indicates that the Earth's surface is moving away from the satellite (i.e., subsidence).

Coherence estimates for the study area can be used to determine the viability of the deformation estimates. Interferometric coherence is a qualitative assessment of the correlation between two SAR images acquired at different times. The degree or lack of coherence controls the feasibility of applying InSAR over the study area, determines the magnitude of phase errors, and thus determines the accuracy of deformation estimates. Constructing a coherent interferogram requires that the SAR images correlate with each other; that is, the backscattering spectrum must be substantially similar over the observation period. Physically, this translates into a requirement that the ground scattering surface be relatively undisturbed at the radar wavelength scale between measurements (Zebker and Villasenor, 1992). Loss of InSAR coherence is also referred to as decorrelation. There are three primary sources of decorrelation: (*i*) thermal decorrelation, caused by the presence of uncorrelated noise sources in radar instruments; (*ii*) spatial decorrelation, which results when the target is viewed from different positions; and (*iii*) temporal decorrelation, caused by environmental changes such as vegetation growth and (or) snow cover. Reduction of radar coherence is the major obstacle to applying InSAR to the Alaska sites, where processes reducing interferometric coherence include snow–ice melting and accumulation, freezing–thawing of surface material, erosion–deposition of

**Table 1.** JERS-1 information relating to the dates of the reference and subordinate images, temporal separation of the reference and subordinate images, the perpendicular baseline for each InSAR pair, the study area imaged by the InSAR pair, and the number of the figure in which the InSAR pair and other information are displayed.

| Reference date | Subordinate date | Temporal separation (days) | Perpendicular baseline (m) | Study site | Figure No. |
|---|---|---|---|---|---|
| 17 June 1996 | 31 July 1996 | 44 | 180 | Kuparuk | 2A, 6A |
| 29 July 1996 | 11 Sept. 1996 | 44 | 9.36 | Cache One Lake | 5A |
| 16 July 1997 | 29 Aug. 1997 | 44 | 1175 | Cache One Lake | Not shown |
| 16 July 1997 | 12 Oct. 1997 | 88 | 1228 | Cache One Lake | 5D |
| 18 July 1997 | 31 Aug. 1997 | 44 | 1228 | Kuparuk | 6D |
| 29 Aug. 1997 | 12 Oct. 1997 | 44 | 507 | Cache One Lake | Not shown |
| 22 May 1998 | 5 July 1998 | 44 | –1419 | Kuparuk | Not shown |
| 3 July 1998 | 16 Aug. 1998 | 44 | 1062 | Cache One Lake | 5G |
| 5 July 1998 | 1 Oct. 1998 | 88 | 1309 | Kuparuk | 6G |
| 6 July 1998 | 2 Oct. 1998 | 88 | 1096 | Kuparuk | Not shown |

**Note:** The perpendicular baseline for all pairs is well within the 5000 m critical baseline for L-band JERS-1 data.

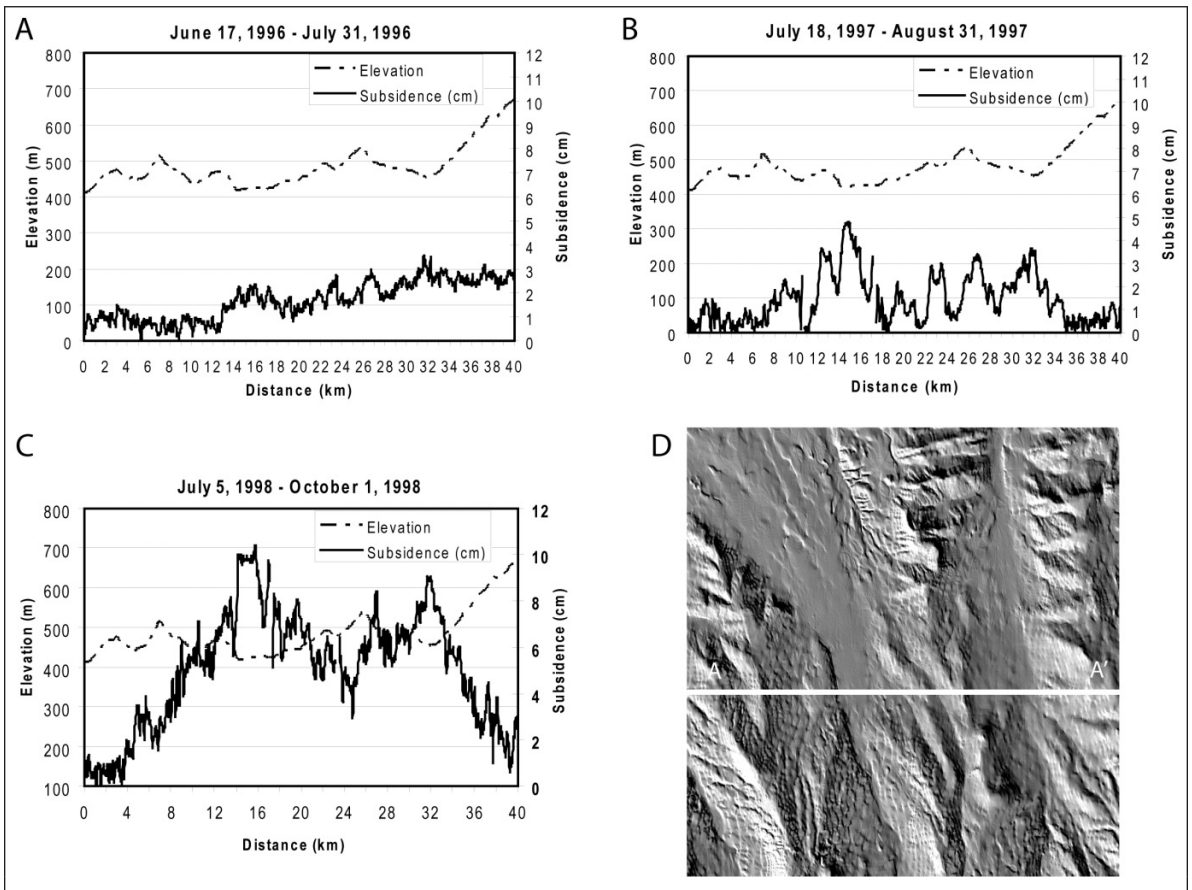


**Figure 4.** (A–C) Profiles from the Kuparuk River study site comparing elevation (broken line) with subsidence (solid line). The elevation and subsidence values were obtained along profile A–A′ as identified in (D). Subsidence values in (A) cover the 44-day period from 17 June to 31 July 1996; subsidence values in (B) cover the 44-day period from 18 July to 31 August 1997; and subsidence values in (C) cover the 88-day period from 5 July – 1 October 1998. Although the subsidence tends to occur along the lowland or riverine areas, all profiles show areas of substantial subsidence occurring in upland areas or in areas with significant slope. This indicates that the USGS DEM was sufficient to remove the effects of topography from the interferograms.

soil, and vegetation change. By analyzing the degree of interferometric coherence over the two study sites, we can better understand whether InSAR is feasible for measuring permafrost-induced deformation over this region.

Three frames of data for each JERS-1 orbit were processed to create an image with an aerial coverage of approximately 90 km × 200 km. During InSAR processing, an anomaly in the phase data of some images appeared as horizontal bands of lost coherence across the scenes (**Figure 2**). The bands of lost coherence, particularly obvious in the phase portion of the interferograms, transect the entire scene and regularly repeat themselves. These bands made processing the complete scene difficult, especially when applying the branch-cut phase unwrapping technique, as it works best when the phase data are contiguous throughout the scene (Goldstein et al., 1988). Focusing on two sites relatively unaffected by the banding problem helped eliminate some of the problems associated with the branch-cut algorithm. Unfortunately, this means that we will not be able to discern any possible subsidence trends occurring over the extent of the entire JERS-1 coverage area (**Figure 2**).

We carefully examined the raw JERS-1 data during processing to ensure that the lines of lost coherence could not be caused by missing lines. First, a scan of the JERS-1 raw data was performed to determine if there were any missing lines in the data by checking the line counter in the header of each line in the raw data. Second, we used the raw data to evaluate the line to line correlation coefficient. If there are any missing lines in the data, the correlation coefficient will be significantly reduced. After applying both procedures, we found no missing lines over the zones of lost coherence. Furthermore, the loss of interferometric coherence over the affected zone, the azimuth offset estimate, and the return of high coherence after the affected zone provide additional evidence to confirm that there were no missing lines in any of the images. These tests boost our confidence that the large offset estimates in the areas of lost coherence are likely due to changes in the total electron content in the ionosphere.

### Ionospheric changes

It has been demonstrated that fluctuations in ionospheric electron density can result in modulations in SAR and InSAR images (Gray et al., 2000; Mattar and Gray, 2002; Meyer et al., 2006; Wegmuller et al., 2006). The ionospheric disturbance in InSAR images could produce an azimuth pixel shift in SAR image correlation and can affect a few kilometres in scale (**Figures 2A**, **2B**). Accordingly, interferometric phase values over the affected region are also biased. The ionospheric effect is more pronounced over polar regions, particularly over strong magnetic disturbance. The effects are more severe on long-wavelength SAR data (e.g., L-band) than on short-wavelength SAR data (e.g., C-band). As L-band JERS-1 SAR data are used in our study area, which reaches to nearly 70°N latitude, we are concerned with any ionospheric delay disturbance in our JERS-1 interferograms.

**Figure 2C** shows the image offsets in azimuth direction by correlating the two SAR images used to produce the interferogram in **Figure 2A**. Azimuth offsets range from –5 to 10 m. This is most likely caused by ionosphere disturbances during SAR image acquisition (Gray et al., 2000; Mattar and Gray, 2002). The ionospheric anomalies affect not only the azimuth offset but also the interferometric phase by introducing phase delays and reducing the coherence of the interferogram. **Figure 2B** is a coherence map with the ionosphere affects. It is obvious the interferometric coherence is lost over the affected zones (cyan). Even though the interferometric coherence can be improved by taking into account the localized offset anomalies (Wegmuller et al., 2006; Yun et al., 2007), the phase anomalies cannot be easily removed. Accordingly, we mask the areas that are severely affected by ionospheric artifacts and do not use the interferometric phase signal over the affected areas for further analysis.

## Analysis and discussion

### Coherence observations: applicability of InSAR

Over the Cache One Lake study site, we produced five usable interferograms from which to draw our observations (**Table 1**). The best coherence between interferometric pairs was obtained with the 44-day repeat pass interferograms (**Figures 5A**, **5G**). However, good coherence was obtained in the 88-day interferogram (**Figure 5D**) covering the period 16 July to 12 October 1997 in all but the alpine areas. The alpine areas in the southeast part of the Cache One Lake study site do not maintain a high degree of coherence, even in the 44-day interferograms, and completely lose coherence in the 88-day interferogram (**Figures 5A**, **5D**, **5G**). The complete loss of coherence in the alpine area in the 88-day interferogram from 1997 (**Figure 5D**) may result from the presence of ice and (or) snow or the diurnal refreezing of the soil in the 12 October 1997 image. The lack of coherence in the alpine areas of the Cache One Lake study site will have little effect on our deformation results, as we expect that the subsidence will be primarily confined to the lowland riverine areas that maintained a high degree of coherence in all interferograms, not just the three shown in **Figure 5**. Also, all five Cache One Lake interferograms were unaffected by the previously mentioned ionospheric problem and the resulting loss of coherence (**Figure 5**).

A total of five interferograms (**Table 1**) provide coverage of the Kuparuk River site. Three of the interferograms have 44-day separations; the other two interferograms have 88-day separations (**Figure 6**). Because of the relative southerly location of the Kuparuk site and its lack of alpine terrain, all interferograms maintained a high degree of coherence (**Figures 6A**, **6D**, **6G**). The northern part of the Kuparuk River site is affected by the banding problem associated with changes in the ionosphere. The interferogram most affected by the banding problem uses data acquired on 6 July and 2 October 1998 (**Table 1**), as the band of lost coherence transects the

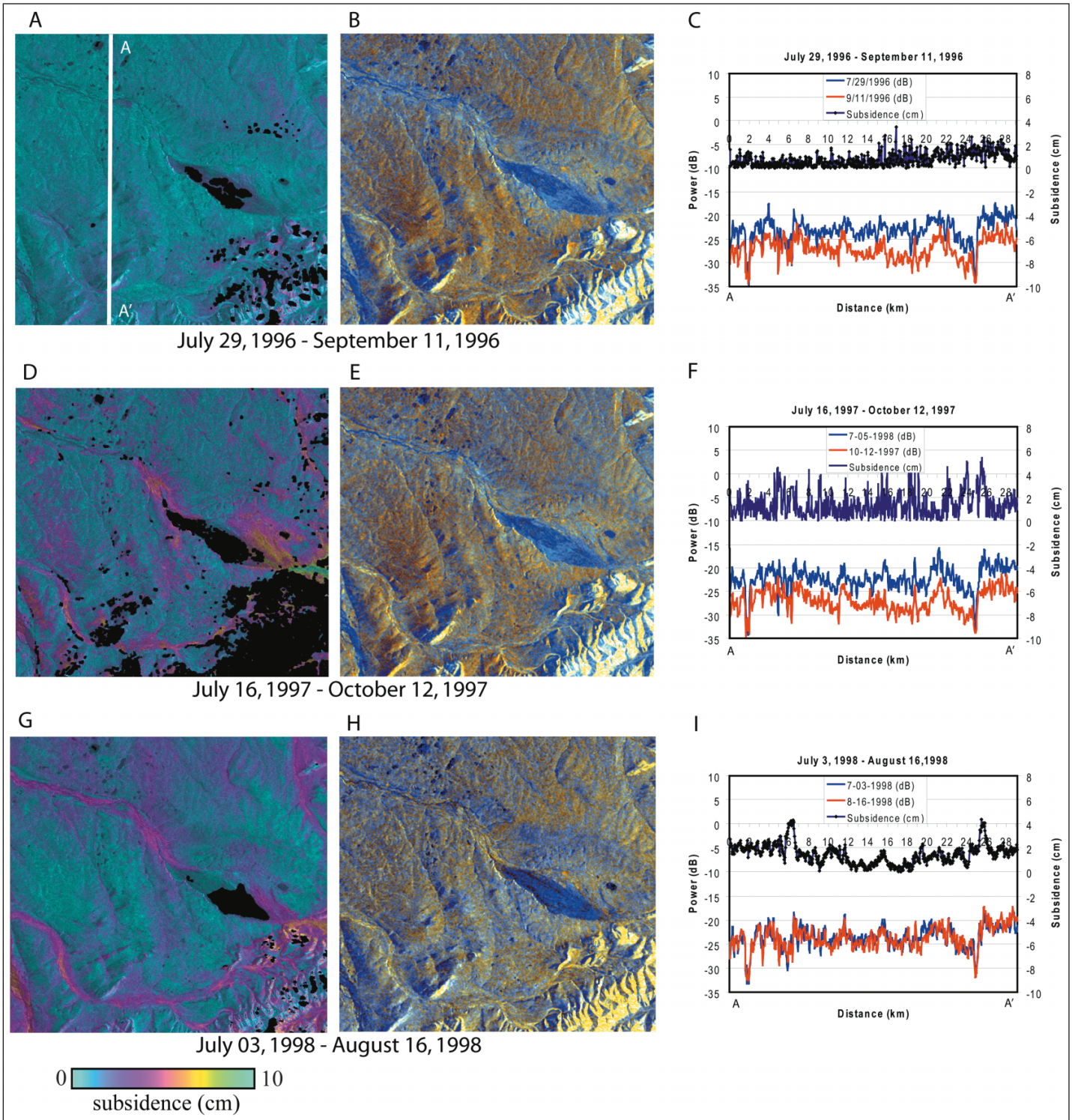


**Figure 5.** Interferograms of subsidence (A, D, G), colorized amplitude images (B, E, H), and subsidence profiles (C, F, I) for the Cache One Lake study site. The interferograms for 1996 (A) and 1998 (G) cover a 44-day period, and the interferogram for 1997 (D) covers an 88-day period. The amount of measured subsidence is valid only between the two image observations and does not represent the total amount of subsidence for the given year. The red–green–blue (RGB) color amplitude composites were created by assigning Power1 to red, Power2 to green, and Power2–Power1 to blue. Subsidence profiles were obtained along the line A–A′ identified in (A), or along a north to south direction. The backscattered intensity or power in (C), (F), and (I) for each image is displayed on the left-hand *y* axis, and the degree of subsidence is displayed on the right-hand *y* axis. A positive deformation change indicates that the surface moved away from the sensor, or surface subsidence.

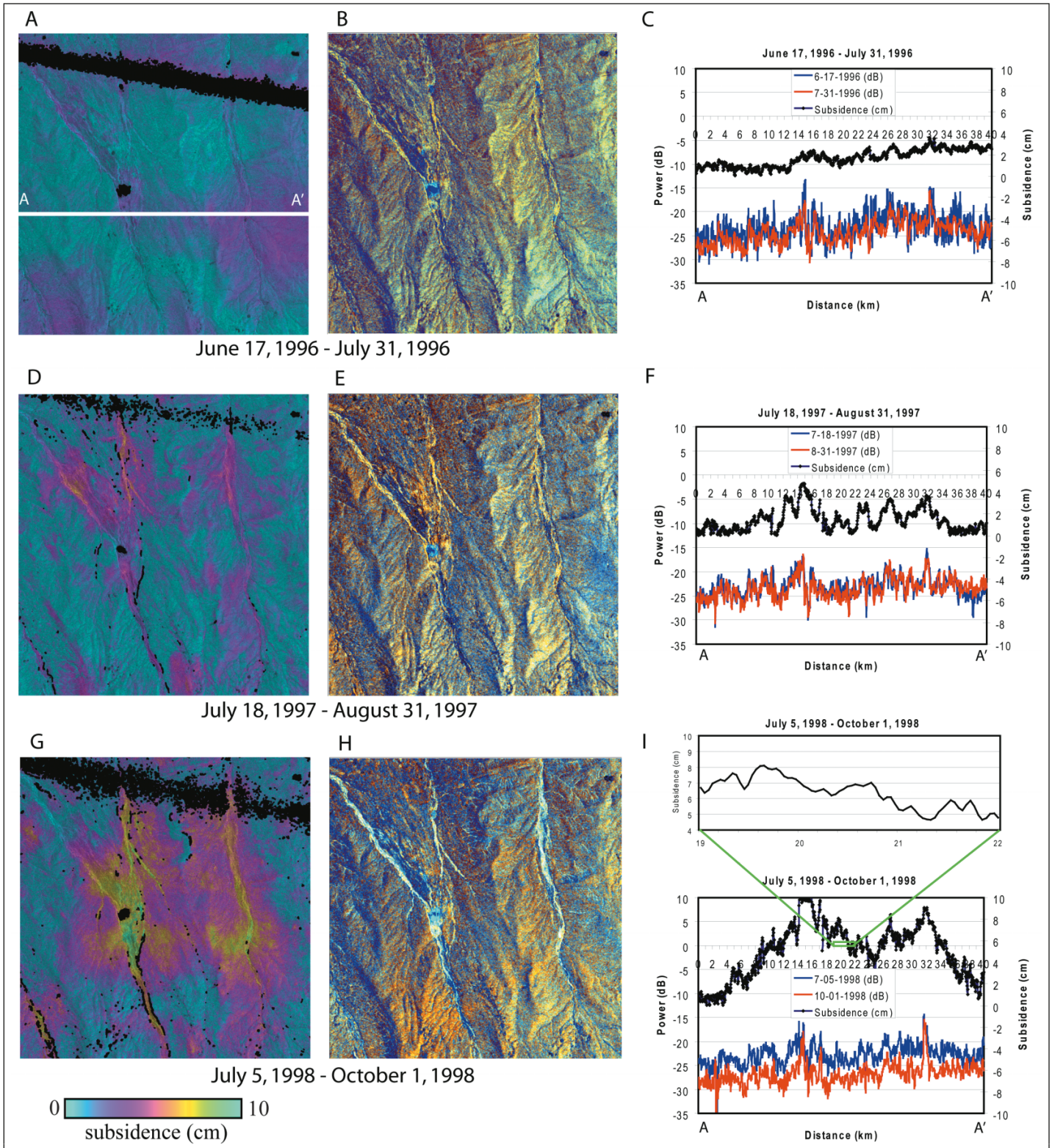


**Figure 6.** Interferograms (A, D, G), colorized amplitude images (B, E, H), and subsidence profiles (C, F, I) for the Kuparuk River study site. The deformation estimates are valid only between the dates of observation between the two InSAR images. Subsidence profiles were obtained along the line A–A′ as identified in (A). The direction of travel of the profiles is east to west. The subsidence estimates for the 1996 and 1997 pairs only cover a 44-day interval, whereas the pair for 1998 covers an 88-day period. Before comparison the interferograms must be normalized to a 44-day period. The colorized radar composites were created by assigning the Power1 to red and Power2 to green; the blue band is the difference of Power2 minus Power1. The profiles (C, F, I) show the image intensity or power on the left-hand *y* axis, and the phase change or subsidence is displayed on the right-hand *y* axis. A positive deformation change indicates that the surface moved away from the sensor, or surface subsidence. To better show the variability of the subsidence estimates, the additional profile in (I) contains an exploded view of the profile from kilometre 19 to kilometre 22.

center of the study site. Another 1998 interferometric pair using imagery collected on 5 July and 1 October 1998 is not as affected by the banding problem and shows good coherence except for the ionospheric contamination in the upper portion of the image (**Figure 6G**). Although the early summer (22 May – 5 July 1998; **Table 1**) interferogram does not exhibit the banding problem, much of the site failed to maintain interferometric coherence, possibly because of the presence of ice, snow, or frozen ground in the 2 May image.

The intermittent lake located near the center of the Kuparuk River study site exhibits seasonal changes, as the coherence of the site fluctuates (**Figures 6A**, **6D**, **6G**). In the 17 June – 31 July 1996 and 5 July – 1 October 1998 interferograms, the area of lost coherence is quite large (**Figures 6A**, **6G**). However, in the late summer to fall interferogram (18 July – 31 August 1997; **Figure 6D**) only a small area has completely lost coherence. The colorized amplitude images in **Figures 6B**, **6E**, and **6H** confirm that the water levels for this small intermittent lake vary throughout the summer and indicate that the lake is likely quite shallow. This rather small area of lost coherence is likely due to the presence of standing water. However, the small intermittent lake and resulting area of lost coherence will not affect the subsidence estimates for the Kuparuk River site, as subsidence can be measured over the broad Kuparuk floodplain.

### Analysis of amplitude data

The JERS-1 backscattered amplitude data, or more succinctly the change in amplitude between two image observations, can be used to help determine a possible source for the deformation. Many radar studies have used the SAR amplitude data to measure changes in soil moisture with varying success (Benallegue et al., 1995; Champion and Faivre, 1997; Dobson and Ulaby, 1981; Hegarat-Mascle et al., 2002; Kane et al., 1996; Ulaby et al., 1996). The colored radar amplitude images for Cache One Lake (**Figures 5B**, **5E**, **5H**) and Kuparuk River (**Figures 6B**, **6E**, **6H**) were created by assigning the reference image to the red band, the subordinate image to the green band, and a difference image (subordinate minus reference) to the blue band. In the difference images, cyan areas have a large positive difference, whereas dark blue areas have a large negative difference. The muted yellow–orange areas in the colored images are indicative of relatively small changes in the backscattered intensity values. If the subsidence in the interferograms were solely due to changes in soil moisture, the colorized amplitude images would reveal patterns of change similar to the subsidence patterns found in the interferograms. Since the patterns found in the colorized amplitude change images for both study sites show no similarity to the deformation patterns in the interferograms, we rule out changes in soil moisture as being the primary driving force behind the deformation. However, changing soil moisture conditions may contribute to the total amount of observed subsidence.

### Thaw settlement – induced subsidence

Analysis of the interferograms is dependant on several critical assumptions: (*i*) the areas experienced no deformation because of tectonic strain; (*ii*) there are no anthropogenic sources of deformation; (*iii*) the L-band JERS-1 is sufficiently long to penetrate the Arctic vegetation; and (*iv*) the elevation of the uplands, with respect to the lowlands, will remain constant. The first assumption, namely that the study area experienced no deformation because of tectonic strain, is met because the area contains no known fault lines. Second, the only possible source of anthropogenic deformation, the National Petroleum Reserve in Alaska, is located too far west of our study site to be of concern. However, Prudhoe Bay, located just north of our study site, is a major source of crude oil. Although the pumping of oil near Prudhoe Bay may lead to deformation in the immediate area, our study sites, located approximately 125 km to the south, should be sufficiently removed from this possible source of contamination. Thus, subsidence associated with oil extraction should not affect our deformation measurements. Our third assumption is that the L-band radar wavelength should be sufficiently long to penetrate the canopy of the short Arctic vegetation, and therefore most of the returned radar signal will be returned as a result of an interaction with the land, rather than the vegetation. Given the 23 cm wavelength of the JERS-1 data and the lack of woody vegetation in our study sites, the JERS-1 radar signal will have no problem penetrating the short Arctic tundra vegetation. Our fourth assumption is that the elevation of the uplands, with respect to the lowlands, will remain relatively constant between JERS-1 acquisitions. Since the depth of the active layer is less in upland areas than in lowland areas, and given that the uplands are underlain by bedrock, the uplands should experience minimal subsidence. If the aforementioned assumptions hold, we assume that most of the remaining deformation signal represents change to the Earth's surface.

The Cache One Lake interferograms for the summers of 1996, 1997, and 1998 (**Figures 5A**, **5D**, **5G**) show varying amounts of land surface subsidence over the site. The 1996 interferogram from 29 July to 11 September 1996 (**Figure 5A**) of Cache One Lake shows little to no deformation, whereas the interferogram from 16 July to 12 October 1997 (**Figure 5D**) shows that about 5 cm of subsidence occurred over the 88-day period, or about 2.5 cm of subsidence over a 44-day period. However, the 44-day interferogram covering the period 3 July to 16 August 1998 (**Figure 5G**) experienced about 4 cm of subsidence. Comparing the 1997 profile (**Figure 5F**) to the 1998 profile (**Figure 5I**) shows that the subsidence along the profile A–A′ for the 1997 interferogram is much more variable than the subsidence in the 1998 interferogram. This large variability might indicate that the 12 October 1997 image was experiencing a daily freeze–thaw cycle or that the area is covered with snow. This would also explain why the 1997 (**Figure 5D**) subsidence is only half that of the 1998 interferogram (**Figure 5G**) and the presence of scattered areas of lost coherence (small black areas) in the interferogram. The

subsidence in the Cache One Lake site for both the 1997 and 1998 interferograms appears to be somewhat constrained by the riverine areas (**Figures 5D**, **5G**), although the area just east of Cache One Lake (magenta to yellow area) exhibits about 6–7 cm of subsidence. Comparing the subsidence patterns in the interferograms for Cache One Lake (**Figures 5A**, **5D**, **5G**) to the vegetation information found in **Figure 3B** reveals that the subsidence is not dependent on vegetation but is located across several vegetation classes. Therefore, we conclude that the effect of the vegetation on the phase signal is negligible.

Given the more southerly location of the Kuparuk River site, we would expect there to be greater subsidence than that observed in the northern Cache One Lake site. Evidence of increased subsidence can be found in the profiles (**Figures 6F**, **6I**) for the 1997 and 1998 interferograms and in the increased number of partial fringes located throughout the interferograms (**Figures 6D**, **6G**). Similar to the 1996 interferogram for Cache One Lake, the 1996 44-day interferogram for the Kuparuk River site shows that only about 2 cm of subsidence occurred in the eastern uplands (**Figure 6A**). The 44-day interferogram covering the period from 18 July to 31 August 1997 shows that about 4–5 cm of subsidence occurred along the Kuparuk River and about 4 cm of subsidence occurred along the riverine system in the eastern part of the scene (**Figure 6D**). Like the Cache One Lake site, the 1998 interferogram for the Kuparuk River exhibits the greatest amount of subsidence (about 10 cm). Normalizing the 88-day interferogram from 5 July to 1 October 1998 to 44-days reveals that the 1997 and 1998 interferograms for the Kuparuk River study site (**Figures 6D**, **6G**) experienced similar amounts of subsidence (**Figures 6F**, **6I**). Whereas the subsidence in the Kuparuk River site was centered over the river channels, the larger floodplain of the river allows for a broader area of deformation. Small amounts of subsidence in the Kuparuk River site are located on upland areas having rather significant amounts of slope and indicates that the topographic effects were removed from the interferograms and that the interferograms were not contaminated by vegetation. It is unlikely that such large amounts of subsidence could be caused solely by the drying of the soil. Instead, the thawing must extend deep into the active layer. However, other hydrologic factors such as the seasonal drying of the active layer and the resulting soil consolidation contribute to the total amount of observed subsidence.

The image acquisition time may affect the amount of observed subsidence in the interferograms. For example, scenes acquired in early spring may be subject to a diurnal freeze–thaw cycle, which may induce subtle, but short-lived surface deformation. Also, lowlands in the Arctic tend to have higher relative humidity levels than the upland areas. High humidity levels in the lowland valleys may cause additional artifacts in the interferogram. These artifacts can be minimized by using multiple interferograms covering similar time periods (Zebker et al., 1997).

## Conclusions

Using all available L-band InSAR data from the JERS-1 sensor, we constructed 16 InSAR pairs acquired during the short Arctic summers of 1996, 1997, and 1998. Ten of those pairs were determined to be relatively free from atmospheric contamination or other noise and were used in our analysis. During construction of the InSAR image pairs we observed a problem with the phase data resulting from changes in the ionosphere that manifests itself as areas of lost coherence laterally transecting the interferograms. Because of ionospheric changes, we were unable to observe any general deformation trends over the entire study area. We were, however, able to work around the strips of lost coherence caused by ionospheric changes by concentrating our efforts on two areas relatively unaffected by the ionospheric changes.

The Cache One Lake and Kuparuk River sites demonstrated various amounts of subsidence, with the least amount of subsidence occurring in the interferograms for 1996 and the maximum amount of subsidence in the 1998 interferograms. For the Cache One Lake site we observed about 4 cm of subsidence near the lake outlet in 1997 and 4–5 cm of subsidence in 1998. For the Kuparuk River site we observed subsidence rates of 4–5 cm in 1997 and about 5 cm in 1998 (when normalized to 44-days). We attribute the greater subsidence rates for the summers of 1997 and 1998 to be primarily because of an increase in the depth to frozen soil resulting from warmer air and ground temperatures and the consequent thawing of ice-rich permafrost in riverine areas. However, other hydrologic properties of permafrost thaw such as the downslope movement of groundwater near the freeze–thaw soil transition and the seasonal drying of the active layer contribute to the total amount of observed subsidence.

Our results provide a promising first step to monitoring thaw subsidence using L-band wavelength JERS-1 InSAR data. Interferograms created from the JERS-1 data maintained sufficient coherence over lowland areas during the 44- and 88-day repeat pass frequency to map subsidence possibly associated with thaw settlement during the short Arctic summers. These results should be treated as preliminary, as the accuracy of the subsidence estimates has not been verified with field measurements.

## Acknowledgments

JERS-1 SAR data are copyright Japan Aerospace Exploration Agency (JAXA), 1996–1998, and were provided by the Alaska SAR Facility (ASF). This study was supported by the USGS Land Remote Sensing Program and USGS Geography Prospectus Fund. We thank ASF User Services for providing the raw JERS-1 SAR signal data and three anonymous reviewers for their insightful comments and thorough reviews.

## References


Bawden, G.W., Thatcher, W., Stein, R.S., Hudnut, K.W., and Peltzer, G. 2001. Tectonic contraction across Los Angeles after removal of groundwater pumping effects. *Nature (London)*, Vol. 412, No. 6849, pp. 812–815.

Benallegue, M., Taconet, O., Vidal-Madjar, D., and Normand, M. 1995. The use of radar backscattering signals for measuring soil moisture and surface roughness. *Remote Sensing of Environment*, Vol. 53, No. 1, pp. 61–68.

Champion, I., and Faivre, R. 1997. Sensitivity of the radar signal to soil moisture: variation with incidence angle, frequency, and polarization. *IEEE Transactions on Geoscience and Remote Sensing*, Vol. 35, No. 3, pp. 781–783.

Christensen, T., Johansson, T., Akerman, J.H., Mastepanov, M., Malmer, N., Friborg, T., Crill, P., and Svensson, B.H. 2004. Thawing sub-arctic permafrost: Effects on vegetation and methane emissions. *Geophysical Research Letters*, Vol. 31, No. L04501.

Dobson, C.M., and Ulaby, F. 1981. Microwave backscatter dependence on surface roughness, soil moisture, and soil texture: Part III – soil tension. *IEEE Transactions on Geoscience and Remote Sensing*, Vol. 19, No. 1, pp. 51–61.

Fialko, Y., Sandwell, D., Agnew, D., Simons, M., Shearer, P., and Minster, B. 2002. Deformation on nearby faults induced by the 1999 Hector Mine earthquake. *Science (Washington, D.C.)*, Vol. 297, No. 5588, pp. 1858–1862. doi:10.1126/science.1074671.

Frohn, R., Hinkel, K.M., and Eisner, W.R. 2005. Satellite remote sensing classification of thaw lakes and drained thaw lakes on the North Slope of Alaska. *Remote Sensing of Environment*, Vol. 97, No. 1, pp. 116–126.

Gesch, D. 1994. *Topographic data requirement for EOS, global change research*. US Geological Survey, Open-file Report 94-626. 60 p.

Goldstein, R.M., Zebker, H.A., and Warner, C.L. 1988. Satellite interferometry: Two dimensional unwrapping. *Radio Science*, Vol. 23, No. 4, pp. 713–720.

Gray, A.L., Mattar, K.E., and Sofko, G. 2000. Influence of ionospheric electron density fluctuations on satellite radar interferometry. *Geophysical Research Letters*, Vol. 27, No. 10, pp. 1451–1454.

Hegarat-Mascle, S.L., Zribi, A.F.M., Weisse, A., and Loumagne, C. 2002. Soil moisture estimation from ERS/SAR data: toward and operational methodology. *IEEE Transactions on Geoscience and Remote Sensing*, Vol. 40, No. 12, pp. 2647–2658.

Hinkel, K.M., and Nelson, F.E. 2003. Spatial and temporal patterns of active layer thickness at Circumpolar Active Layer Monitoring (CALM) sites in northern Alaska, 1995–2000. *Journal of Geophysical Research*, Vol. 108, No. D2, p. 8168. doi:10.1029/2001JD000927.

Hinkel, K.M., Outcalt, S.I., and Nelson, F.E. 1990. Temperature variation and apparent thermal diffusively in the refreezing active layer, Toolik Lake, Alaska. *Permafrost and Periglacial Processes*, Vol. 1, No. 3–4, pp. 265–274.

Hinkel, K.M., Paetzold, F., Nelson, F.E., and Bockheim, J.G. 2001. Patterns of soil temperature and moisture in the active layer and upper permafrost at Barrow, Alaska: 1993–1998. *Global and Planetary Change*, Vol. 29, No. 3–4, pp. 293–309. doi:10.1016/S0921-8181(01)00096-0.

Hinkel, K.M., Eisner, W.R., Bockheim, J.G., Nelson, F.E., Peterson, K.M., and Dai, X. 2003. Spatial extent, age, and carbon stocks in drained thaw lake basins on the Barrow Peninsula, Alaska. *Arctic, Antarctic, and Alpine Research*, Vol. 35, No. 3, pp. 291–300.

Hinzman, L.D., Kane, D.L., Gieck, R.E., and Everett, K.R. 1991. Hydrologic and thermal properties of the active layer in the Alaskan Arctic. *Cold Regions Science and Technology*, Vol. 19, No. 2, pp. 95–110.

Jorgenson, M.T., and Heiner, M. 2004. *Map of ecosystems of northern Alaska*. ABR, Inc., Fairbanks, Alaska, and The Nature Conservancy, Anchorage, Alaska. Available from www.uspermafrost.org/reports/NoAK_Ecosystems_tabloid_med.pdf

Jorgenson, M.T., Racine, C.H., Walters, J.C., and Osterkamp, T.E. 2001. Permafrost degradation and ecological changes associated with a warming climate in central Alaska. *Climate Change*, Vol. 48, No. 4, pp. 551–579.

Jorgenson, M.T., Shur, Y.L., and Pullman, E.R. 2006. Abrupt increase in permafrost degradation in Arctic Alaska. *Geophysical Research Letters*, Vol. 33, No. L02503. doi:10.1029/2005GRL024960.

Kane, D.L., Hinzman, L.D., Yu, H., and Goering, D.J. 1996. The use of SAR satellite imagery to measure active layer moisture contents in Arctic Alaska. *Nordic Hydrology*, Vol. 27, No. 1–2, pp. 25–38.

Lawrence, D.M., and Slater, A.G. 2005. A projection of severe near-surface permafrost degradation during the 21st century. *Geophysical Research Letters*, Vol. 32, No. L24401. doi:10.1029/2005GL02080.

Little, J.D., Sandall, H., Walegur, M.T., and Nelson, F.E. 2003. Application of Differential Global Positioning Systems to monitor frost heave and thaw settlement in tundra environments. *Permafrost and Periglacial Processes*, Vol. 14, No. 4, pp. 349–357.

Lu, Z. 2007. InSAR imaging of volcanic deformation over cloud-prone areas — Aleutian Islands. *Photogrammetric Engineering & Remote Sensing*, Vol. 73, No. 3, pp. 245–257.

Lu, Z., Masterlark, T., Dzurisin, D., Rykhus, R., and Wicks, C. 2003. Magma supply dynamics at Westdahl volcano, Alaska, modeled from satellite radar interferometry. *Journal of Geophysical Research*, Vol. 108, No. B7. doi:10.1029/2002JB002311.

Lu, Z., Crane, M., Kwoun, O.-I., Wells, C., Swarzenski, C., and Rykhus, R. 2005a. C-band radar observes water level change in swamp forests. *EOS Transactions, American Geophysical Union*, Vol. 86, No. 14, pp. 141–144.

Lu, Z., Masterlark, T., and Dzurisin, D. 2005b. Interferometric synthetic aperture radar study of Okmok volcano, Alaska, 1992–2003: Magma supply dynamics and postemplacement lava flow deformation. *Journal of Geophysical Research*, Vol. 110, No. B2. doi:10.1029/2004JB003148.

Lu, Z., Wicks, C., Kwoun, O., Power, J.A., and Dzurisin, D. 2005c. Surface deformation associated with the March 1996 earthquake swarm at Akutan Island, Alaska, revealed by C-band ERS and L-band JERS radar interferometry. *Canadian Journal of Remote Sensing*, Vol. 31, No. 1, pp. 7–20.

Lu, Z., Dzurisin, D., Wicks, C., Power, J., Kwoun, O., and Rykhus, R. 2007. Diverse deformation patterns of Aleutian volcanoes from satellite interferometric synthetic aperture radar (InSAR). In *Volcanism and subduction: the Kamchatka region*. Edited by J. Eichelberger, E. Gordeev, M. Kasahara, P. Izbekov, and J. Lees. American Geophysical Union, Washington, D.C. Geophysical Monograph 172, pp. 249–261.

Massonnet, D., and Feigl, K. 1998. Radar interferometry and its application to changes in the Earth's surface. *Reviews of Geophysics*, Vol. 36, No. 4, pp. 441–500.

Mattar, K.E., and Gray, A.L. 2002. Reducing ionospheric electron density errors in satellite radar interferometry applications. *Canadian Journal of Remote Sensing*, Vol. 28, No. 4, pp. 593–600.

McNamara, J.P., Kane, D.L., and Hinzman, L.D. 1998. An analysis of streamflow hydrology in the Kuparuk River Basin, Arctic Alaska: a nested watershed approach. *Journal of Hydrology*, Vol. 206, No. 1–2, pp. 39–57.

Meyer, F., Bamler, R., Jakowski, N., and Fritz, T. 2006. The potential of low-frequency SAR systems for mapping ionospheric TEC distributions. *IEEE Geoscience and Remote Sensing Letters,* Vol. 3, No. 4, pp. 560–564.

Nelson, F.E., Shiklomanov, N.I., Mueller, G.R., Hinkel, K.M., Walker, D.A., and Bockheim, J.G. 1997. Estimating active-layer thickness over a large region: Kuparuk River basin, Alaska, U.S.A. *Arctic and Alpine Research*, Vol. 29, No. 4, pp. 367–378.

Nelson, F., Hinkel, K., Shiklomanov, N., Mueller, G., Miller, L., and Walker, D. 1998. Active-layer thickness in north central Alaska: Systematic sampling, scale, and spatial autocorrelation. *Journal of Geophysical Research*, Vol. 103, No. D22, pp. 28 963 – 28 973.

Nelson, F.E., Anisimov, O.A., and Shiklomanov, N.I. 2002. Climate change and hazard zonation in the circum-arctic permafrost regions. *Natural Hazards*, Vol. 26, No. 3, pp. 203–225. doi:10.1023/A:1015612918401.

Oechel, W.C., Vourlitis, G.L., Hastings, S.J., Zulueta, R.C., Hinzman, L., and Kane, D. 2000. Acclimation of ecosystem $CO_2$ exchange in the Alaskan Arctic in response to decadal climate warming. *Nature (London)*, Vol. 406, No. 6799, pp. 978–981.

Pullman, E.R., Jorgenson, M.T., and Shur, Y. 2007. Thaw settlement in soils of the Arctic Coastal Plain, Alaska. *Arctic, Antarctic and Alpine Research*, Vol. 39, No. 3, pp. 468–476. doi:10.1657/1523-0430(05-045)[PULLMAN]2.0.CO;2.

Rosen, P., Hensley, S., Zebker, H., Webb, F., and Fielding, E.J. 1996. Surface deformation and coherence measurements of Kilauea volcano, Hawaii, from SIR-C radar interferometry. *Journal of Geophysical Research*, Vol. 101, No. E10, pp. 23 109 – 23 126. doi:10.1029/96JE01459.

Shiklomanov, N.I., and Nelson, F.E. 1999. Analytic representation of the active layer thickness field, Kuparuk River Basin, Alaska. *Ecological Modelling*, Vol. 123, No. 2–3, pp. 105–125.

Tarnocai, C. 2004. Organic carbon in cryosolic soils in the Northern Circumpolar Region. *Frozen Ground*, No. 28, pp. 6–7.

Ulaby, F.T., Dubois, P.C., and Zyl, J.v. 1996. Radar mapping of surface soil moisture. *Journal of Hydrology*, Vol. 184, pp. 57–84.

Walker, M.D., Walker, D.A., and Auerbach, N.A. 1994. Plant communities of a tussock tundra landscape in the Brooks Range foothills, Alaska. *Journal of Vegetation Science*, Vol. 5, No. 6, pp. 843–866.

Walter, K.M., Zimo, S.A., Chanton, J.P., Verbyla, D., and Chapin, F.S. 2006. Methane bubbling from Siberian thaw lakes as a positive feedback to climate warming. *Nature (London)*, Vol. 443, No. 7, pp. 71–75. doi:10.1038/nature05040.

Wang, Z., and Li, S. 1999. Detection of winter frost heaving of the active layer of arctic permafrost using SAR differential interferograms. In *IGARSS'99: Proceedings of the International Geoscience and Remote Sensing Symposium*, 28 June – 2 July 1999, Hamburg, Germany.

Wegmuller, U., Werner, C., Strozzi, T., and Wiesmann, A. 2006. Ionospheric electron concentration effects on SAR and INSAR. In *IGARSS'06: Proceedings of the International Geoscience and Remote Sensing Symposium*, 24–29 July 2006, Denver, Colo. doi:10.1109.IGARSS.2006.956.

Wicks, C., Jr., Thatcher, W., and Dzurisin, D. 1998. Migration of fluids beneath Yellowstone Caldera inferred from satellite radar interferometry. *Science (Washington, D.C.)*, Vol. 282, No. 5388, pp. 458–462. doi:10.1126/science.282.5388.458.

Yun, S.H., Zebker, H., Segall, P., Hooper, A., and Poland, M. 2007. Interferogram formation in the presence of complex and large deformation. *Geophysical Research Letters*, Vol. 34, No. L12305. doi:10.1029/2007GL029745.

Zebker, H., and Villasenor, J. 1992. Decorrelation in interferometric radar echoes. *IEEE Transactions on Geoscience and Remote Sensing*, Vol. 30, pp. 950–959.

Zebker, H., Rosen, P., and Hensley, S. 1997. Atmospheric effects in interferometric synthetic aperture radar surface deformation and topographic maps. *Journal of Geophysical Research*, Vol. 102, pp. 7547–7563.

Zhang, T., Barry, R.G., Knowles, K., Heginbottom, J.A., and Brown, J. 1999. Statistics and characteristics of permafrost and ground-ice distribution in the Northern Hemisphere. *Polar Geography*, Vol. 23, pp. 132–154.